Analyst

Check for updates

On-chip hydrodynamic chromatography of DNA through centimeters-long glass nanocapillaries†

Lian Duan[a] and Levent Yobas [ID] *[a,b]

This study demonstrates hydrodynamic chromatography of DNA fragments in a microchip. The microchip contains a highly regular array of nanofluidic channels (nanocapillaries) that are essential for resolving DNA in this chromatography mode. The nanocapillaries are self-enclosed robust structures built inside a doped glass layer on silicon using low-resolution photolithography and standard semiconductor processing techniques. Additionally, the unique nanocapillaries feature a cylindrical inner radius of 600 nm maintained over a length scale of 5 cm. The microchip with bare open nanocapillaries is shown to rapidly separate a digest of lambda DNA in free solution (<5 min under the elution pressure of 60 to 120 psi), relying entirely on pressure-driven flows and, in doing so, avoiding the field-induced DNA aggregations encountered in gel-free electrophoresis. The nanocapillaries, despite their relatively short length, are observed to fractionate DNA fragments reasonably well with a minimum resolvable size difference below 5 kbp. In the chromatograms obtained, the number of theoretical plates exceeds 10^5 plates per m for 3.5 and 21 kbp long DNA fragments. The relative mobility of fragments in relation to their size is found to be in excellent agreement with the simple quadratic model of hydrodynamic chromatography. The model is shown to estimate greater effective hydrodynamic radii than those of respective fragments being unconfined in bulk solution, implying increased drag forces and reduced diffusion coefficients, which is also a noticeable trend among diffusion coefficient estimates derived from the experimentally obtained plate heights. This robust mass-producible microchip can be further developed into a fully integrated bioanalytic microsystem.

Introduction

The separation and analysis of DNA play a crucial role in basic research and clinical diagnosis.[1] For decades, various forms of electrophoresis techniques including pulsed-field gel electrophoresis (PFGE) and capillary gel electrophoresis (CGE) have been utilized as the workhorse of DNA analysis.[2–4] In recent years, however, extensive research efforts have been devoted to gel-free approaches with the advent of a miniaturization trend as well as the notion of distributed analysis of clinical samples.[5] Apart from the desire to advance DNA analysis (*e.g.*, resolution, speed), a major drive in these efforts has been the challenge of introducing viscous gel matrixes into miniaturized platforms. Nevertheless, electrophoresis in a gel-free solu-

tion can only resolve short fragments (≲400 bp) since the electrophoretic mobility becomes independent of the fragment size beyond this range.[6]

Artificial sieving matrixes as opposed to conventional disordered gels present a highly ordered pore array defined through lithographic patterning or templating of self-assembled beads.[7,8] Many of these matrixes can be readily integrated into miniaturized units for DNA analysis. The prominent ones include micrometer- or nanometer-scale post arrays,[9,10] colloidal crystals,[11] and, more recently, three-dimensional structures of nanowires[12] and arrays of alternating nanocapillaries (or nanoslits) and wells.[13–15] DNA fragments migrating in the slit-well or capillary-well topology repeatedly experience one- or two-dimensional nanometer-scale periodic confinements that can be fabricated through low-resolution photolithography. The capillary-well motif, with the virtue of higher-dimensional confinement, supports electrophoresis at fairly high voltages without facing breakdown in the sieving mechanism, thereby advancing the separation speed without compromising the resolving power.[14,15] Nevertheless, high voltages that are essential for the electrophoresis speed and resolution induce strong aggregation of large DNA chains and render effective sieving through these structures impractical.[16]

*[a]Department of Electronic and Computer Engineering, The Hong Kong University of Science and Technology, Clear Water Bay, Hong Kong SAR, China.
E-mail: eelyobas@ust.hk; Fax: +852 2358 1485; Tel: +852 2358 7068
[b]Division of Biomedical Engineering, The Hong Kong University of Science and Technology, Clear Water Bay, Hong Kong SAR, China*

Pressure-driven size separation of DNA chains in miniaturized platforms has been explored rarely, although reports are available on the hydrodynamic-field-driven interactions of DNA chains with microscopic posts or pits at the single molecule level.[17,18] Individual DNA molecules undergoing pressure-driven transport through nanoslits have also been studied by fluorescence microscopy revealing the mobility and effective diffusivity of chains in confined spaces which are fundamental to the chip-based hydrodynamic chromatography (HDC) of DNA.[19] The scarcity of reports on this approach could be in part due to the convenience of performing separation in miniaturized platforms through voltage as opposed to pressure from an engineering point of view (*e.g.*, fluidic interfacing). Moreover, chromatographic methods are generally considered inferior to those electrophoretic approaches in resolving power. Very recently, however, Wang and colleagues, using open tubular bare silica nanocapillaries (inner radius ≲1 μm), demonstrated pressure-driven gel-free separation of DNA molecules at an unprecedented combination of high resolution and wide dynamic size range.[20] The authors attributed their results to HDC as well as transverse electromigration of DNA across the electric double layer (EDL) near the capillary wall.[21] While the latter is influential on short DNA strands, the former concerns comparatively long chains. This approach, which was later adopted for single-molecule DNA analysis,[22] is simple and effective compared to a previously introduced gel-free method in which wide capillaries are used instead for separating large DNA chains under a combined action of pressure-driven flow and electrophoresis.[23] Discrete fused-silica capillaries, however, have been used in all these pioneering studies and to date no demonstration of pressure-driven size separation of DNA has been made using a miniaturized integrated platform (microchip). Microchips offer an integrated sample injector and separation capillary using minimal dead volume. This integration is crucial for the overall separation performance through enhancing sample injection efficiency, *i.e.*, leakage-free volume-defined and reproducible injection of a short sample band.[24]

In this work, we present experimental results on pressure-driven size separation of DNA chains through open tubular bare glass nanocapillaries integrated on a robust silicon-based microchip (Fig. 1A). The nanocapillaries are fabricated through low-resolution photolithography and they feature a cylindrical interior inside a monolithic glass layer and present a smooth surface finish being free of etch defects; hence, the resemblance to fused-silica capillaries used in aforementioned studies.[25] Fig. 1B shows the method of fabrication, which also considerably departs from the well-known methods of forming nanochannels. The fabrication leverages shadowing-based deposition of a doped glass layer that leads to self-enclosed channels inside centimeters-long rectangular silicon trenches imprinted with a relatively coarse mask pattern (critical dimension ≳3 μm). The fabrication also leverages a thermal reflow process that transforms the self-enclosed channels from triangular to cylindrical tubes featuring an inner radius of ~600 nm.[26] The capillary radius can be further scaled down
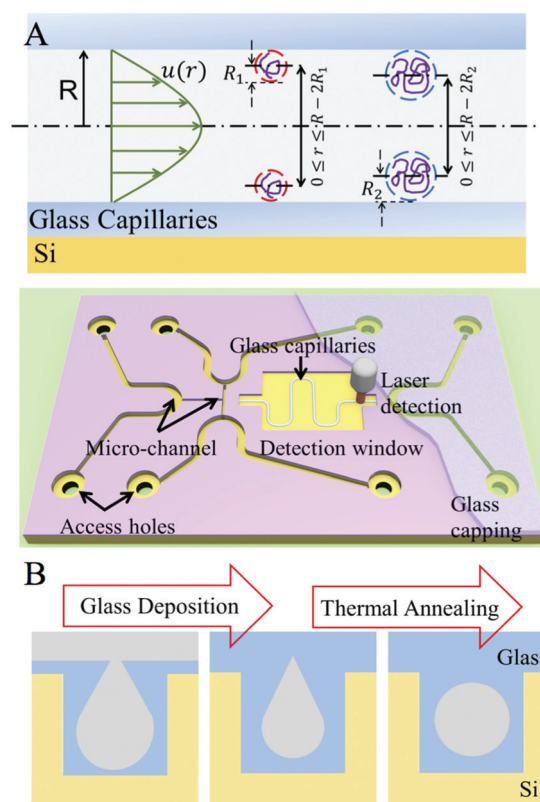

Fig. 1 Illustrations: (A) the principle of hydrodynamic chromatography (HDC) described for the size resolving DNA fragments through a nano-capillary with a radius $R \lesssim 1$ μm (longitudinal view, upper panel) and 3D rendering of the microchip; (B) critical steps involved in the integration of the self-enclosed cylindrical nanocapillary inside silicon trenches (cutaway views). The function $u(r)$ represents the pressure-driven parabolic flow velocity profile.

controllably below 50 nm by extending the reflow duration.[15,26] However, this is undesired here because nanoslit experiments revealed that the pressure-driven mobility of DNA becomes independent of the chain length when the slit height is below 1 μm.[19] Moreover, unlike the recent demonstration of centimeters-long integrated nanochannels for femtoliter liquid chromatography of fluorescent dyes,[27] the capillary integration does not demand low-throughput advanced lithography tools. Furthermore, the self-forming cylindrical capillary profile in relation to the rectangular nanochannel geometry might lead to an enhanced separation resolution according to our experimental results on the pressure-driven chromatography modes in nanochannels featuring distinct cross-sectional profiles.[25]

Experimental

Device

All the devices were fabricated using standard semiconductor processing tools and low-resolution photolithography. The process is further described in the ESI text and Fig. S-1 (see the ESI†).

Pneumatics

Sequential steps of sample analyte injection and separation in nanocapillaries were realized through a custom-built automated pneumatic system (ESI text and Fig. S-2†). The sample mixture and the elution buffer were delivered from pressurized liquid tanks through PTFE tubings directly into the microchip. The microchip was sandwiched inside a machined stainless steel holder with a set of access ports, to which PTFE tubings were connected *via* Nanoport fittings (IDEX Health & Science, Oak Harbor, WA).

Reagents

A mixed digest of *Eco*RI-cut λ-DNA (3530–21 226 bp) was acquired from Sigma-Aldrich (St Louis, MO). DNA fragments were stained with an intercalating dye, YOYO-1 (Thermo Fisher Scientific, Waltham, MA) at a dye-to-base-pair ratio of 1:10 and further diluted to a final concentration of ~50 μg mL^{-1} in 1× TE buffer containing 10 mM Tris, and 1 mM EDTA (pH, 8.0). The pH was measured with a pH meter (Mettler Toledo, Inc., OH) and further adjusted by adding HCl.

Measurements

All the experiments were observed under an epifluorescence microscope (Eclipse, Nikon, Tokyo, Japan) equipped with a solid-state laser at 488 nm for excitation and a filter cube set for detection (ex/em in nm: 492/520). Time-series images of fluorescence bands were captured using an EMCCD camera (iXon3897, Andor) and then analysed by using software ImageJ (NIH, Bethesda, MD). The chromatograms were generated by plotting the measured fluorescence intensities from a select region of interest (ROI ~ 2 μm by 2 μm) at a position about 600 μm before the nanocapillaries end. The chromatogram peaks were fitted with Gaussians to acquire the required parameters for each peak, including the retention time t_R, the base width in units of time w_b, and the peak variance $σ$ (OriginPro 9.0, OriginLab Corporation, Northampton, MA). These fittings were used in the assessment of the number of theoretical plates N, and the height equivalent to a theoretical plate H, according to the relations $N = 16(t_R/w_b)^2$ and $H = L_{eff}/N$ with L_{eff} being the effective separation length (~4.94 cm). The separation resolution R_s between two peaks (*e.g.*, peak 1 and peak 2) was evaluated according to the formula $R_s = 2(t_{R,1} - t_{R,2})/(w_{b,1} + w_{b,2})$.

Results and discussion

Microchip

Fig. 2A depicts a representative microchip in a layout view. Four microchannels in the U-shape design are seen partially. A pair of fluidic ports addresses each microchannel with one serving as the exit port for bubble release during device priming. All the release ports are blocked throughout the microchip operation. The channels are enclosed from above with a glass cover plate placed over the entire substrate. The substrate surface, except within the observation window, is
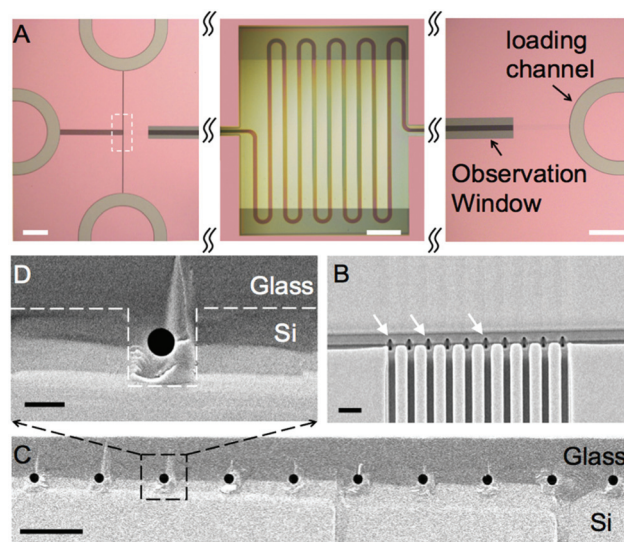

Fig. 2 Images of a representative microchip. (A) Plan view (fluidic ports left outside the field of view). The detection window defined through the amorphous silicon film allows the sight of the nanocapillary array (total 10). The nanocapillaries are in a serpentine shape and 5 cm long measured with reference to the sample injection junction (the dashed box). (B) The sample injection junction depicted from an oblique view revealing the nanocapillary openings (arrows). (C) The nanocapillary array depicted from a sectioned view exposing its highly ordered profile (radius: 600 nm). (D) Close-up shot of a single nanocapillary. Scale bars: (A) 400 μm (center panel: 1 mm); (B, C) 10 μm; and (D) 2 μm.

coated with thin-film amorphous silicon, which is opaque and conceals the self-enclosed nanocapillaries. However, this thin film is required for the success of anodic bonding in securing a cover plate in place despite the thick dielectric (doped glass) layer underneath.

Fig. 2B presents the sample injection junction from an oblique view. The self-enclosed nanocapillary openings can be seen with each opening opposing a trench, 5 μm wide and deep and 1 mm long, which is an extension of a microchannel that supplies the elution buffer concurrently to all. The trench that runs orthogonal to the nanocapillaries extends on either side 1 mm long and 5 μm wide and deep to a microchannel for loading the sample analyte or collecting the sample waste. The microchip features an array of self-enclosed nanocapillaries (total 10) highly ordered in shape (round) and size (radius 600 nm) as revealed by the cutaway image shown in Fig. 2C. Fig. 2D depicts an image closing up on a single nanocapillary within the array.

Sample plug injection

A "pinched-injection" scheme was adopted as illustrated in Fig. 3A.[28] A custom-built pneumatic system (Fig. S-2†) capable of switching supply pressure rapidly (minimum ~10 ms) was utilized for the precision injection of a short sample band into the nanocapillaries. Sequential steps of sample loading, injection, and band formation were executed on the microchips
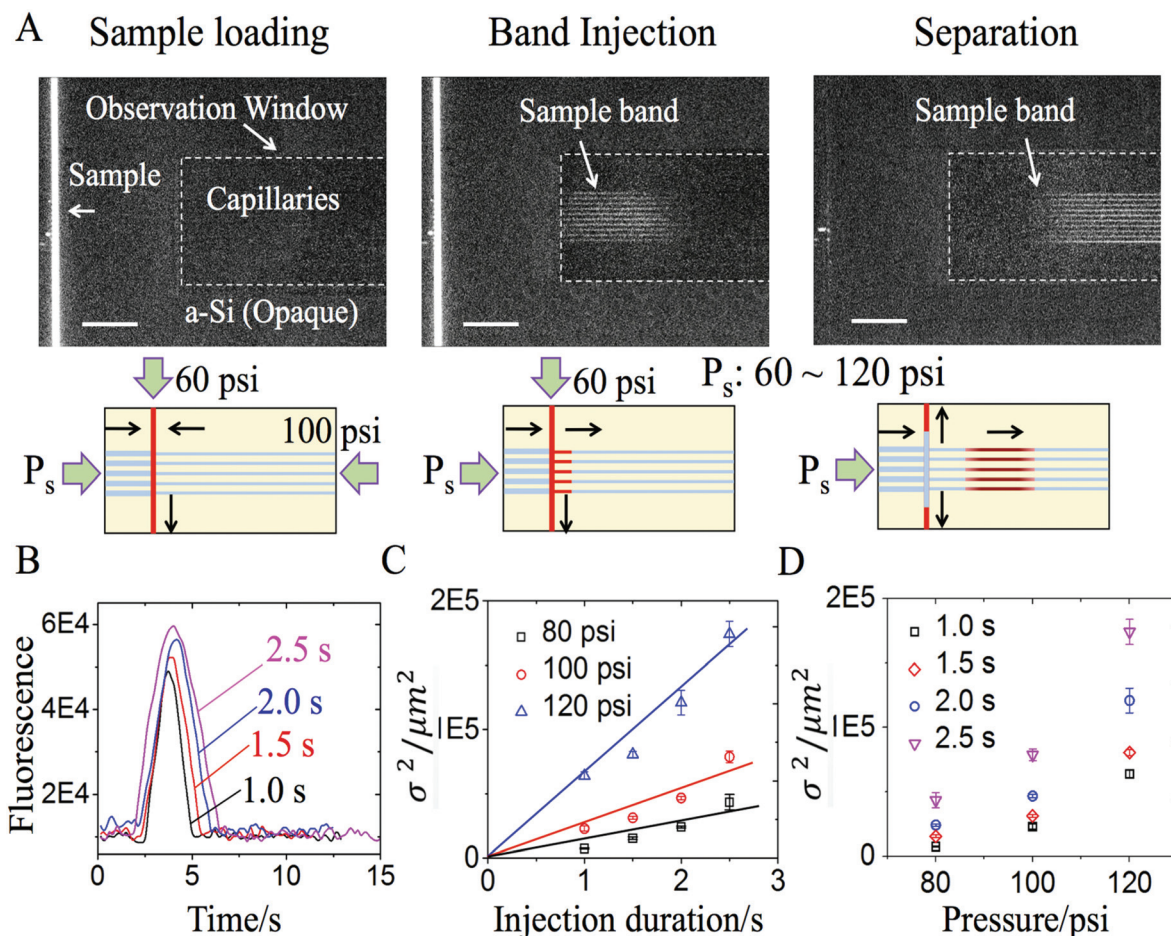
Fig. 3 Sample injection. Pressure-driven pinched injection scheme: (A) fluorescence images and corresponding schematics of the injection junction being integrated with the nanocapillaries. (B) Chromatograms of the formed bands with the injection step applied for various set durations (all at 100 psi). (C and D) Band variance (C) against the injection duration under various set pressures and (D) against the injection pressure for various set durations. Scale bars: 200 μm.

being completely filled with the elution buffer. The applied pressure protocol to realize these steps is further described in schematics and fluorescence images shown in Fig. 3A. During sample loading, the sample waste outlet was left open to the atmosphere while all the fluidic ports were pressurized. Subsequent release of pressure first at the elution waste outlet and then at the sample inlet initiated and terminated the application of a brief sample injection step, forming the sample band. The band was driven into separation along the nanocapillaries by maintaining the elution inlet pressure at the applied level (at the injection pressure).

The sample injection duration is a crucial parameter since it determines the sample band size. A short sample band, while desirable to achieve a high efficiency separation (low plate heights), is usually associated with a low intensity peak that is difficult to detect. Subsecond injection durations failed to generate bands that can be detected further downstream along the nanocapillaries. By increasing the injection duration from 1 to 2.5 s, the sample volume introduced into the nanocapillaries under 100 psi varied from ~300 to 700 fL,

which is fairly small in comparison with those reported for discrete fused-silica nanocapillaries.[21,29] We also quantitatively analyzed the sample band variance based on the chromatograms obtained from the nanocapillaries near the injection junction (Fig. 3B). In Fig. 3C and D, the plots show more or less linear trends between the variance of the band and the injection duration ($R^2 > 0.97$, under a constant injection pressure: 80, 100, and 120 all in psi) as well as the injection pressure ($R^2 \sim 0.95$, for a constant injection duration: 1, 1.5, 2, and 2.5 all in s). These linear trends follow the Poiseuille relation, $\Delta V = \Delta P \pi R^4 \Delta t / 8 \mu L$, where ΔV is the injected sample volume, ΔP and Δt are the injection pressure and duration, R and L are the capillary radius and length, and μ is the viscosity. The linear trends also suggest that the sample band volume can be quantitatively controlled with accuracy by modulating ΔP and Δt. In subsequent experiments, the band variance plots were used as a guide for adjusting the injection duration such that a comparable sample volume (or a sample band length) was introduced each time regardless of the pressure.

HDC separation of DNA

We used a mixture of *Eco*RI-cut λ-phage DNA with six fragments, 3530 to 21 226 bp long and with the corresponding hydrodynamic radii (R_{HD}) ~100 to ~300 nm in bulk solution. A band of the mixture at a concentration of 50 μg mL^{-1} in TE buffer (10 mM) was introduced into the nanocapillaries following the described injection protocol and then separated under an elution pressure applied within the range of 60 to 120 psi.

Fig. 4 displays the chromatograms detected at a site ~600 μm away from the capillary end. Under an elution pressure of 60 psi, the mixture can be found to be size separated into the corresponding peaks in less than 5 min except for the fragments 5.6 and 5.8 kbp. Nanocapillaries longer than 5 cm are required to resolve fragments that are only separated by a small difference (≲200 bp). However, the nanocapillary length here is adequate to resolve fragments of 21- and 7.4 kbp, suggesting a minimum resolvable size difference of ~4.9 kbp which is evaluated by normalizing the differential size of the fragments with their peak resolution (R_s ~ 2.8). Interestingly, the minimum resolvable size difference accord-

ing to the fragments 4.8 and 3.5 kbp is even smaller (~1.6 kbp; R_s ~ 0.8). It is likely that relatively large chains being more deformable assume an elongated conformation under the applied shear whereas smaller chains that have R_{HD} about thrice the persistence length closely emulate rigid spheres featured in the hydrodynamic model.[29,30] By comparison, the minimum resolvable size difference achieved previously in discrete fused-silica capillaries at a slightly larger radius (750 nm) and yet much larger length (42 cm) is 100 bp.[29] However, this was attained at an elution pressure of 100 psi and with a considerably prolonged elution time (~1 h) due to the substantial flow resistance exerted by long capillaries. Increasing the elution pressure from 60 to 120 psi enhanced the separation rate at the expense of resolution, reducing the total time from 5 to ~2 min with the entire elution window realized in ~30 s. The capillary diameter plays an important role in resolving DNA fragments in this chromatography mode. By comparison, HDC in a 5 μm i.d. fused-silica capillary failed to fractionate fragments ranging from 10 to 50 kbp which eluted together as a single peak after a 45 cm run under 1 psi cm^{-1}.[31]

Separation mechanism

To further establish HDC as the separation mechanism, we evaluated the relative mobility of DNA fragments $\bar{\mu}_L$ in relation to the fragment length N_{kbp} in kbp and found the relation to be in close agreement with the HDC quadratic model:[30]

$$
\begin{aligned}
\bar{\mu}_L &= \bar{u}_L/\bar{u} = 1 + 2\lambda - \lambda^2 \\
\lambda &= R_{HD}/R \\
R_{HD} &= kN_{kbp}^{\nu}
\end{aligned}
\tag{1}
$$

where $\bar{u}_L$ and $\bar{u}$ represent the average velocity of fragments and of the mobile phase, respectively, R_{HD} the hydrodynamic radius of DNA with ν and k being the scaling exponent and prefactor, and R the nanocapillary radius (600 nm). For self-avoiding persistent polymers, the scaling exponent is assigned to be 0.6,[32,33] whereas for ideal non-self-avoiding polymers, ν = 0.5.[34] The average fragment velocity $\bar{u}_L$ is taken as the effective separation length divided by the retention time of fragments of a specific length N_{kbp} and with each fragment regarded as a solid sphere at a relative radius λ. The average buffer velocity $\bar{u}$ is determined here based on the retention time of fluorescein bands which independently run through the nanocapillaries (Fig. S-3†). In those measurements, a high ionic strength buffer (10 mM Tris) was used to suppress the capillary wall EDLs and their field-effect influence on the distribution of fluorescein species.

Fig. 5A shows a plot of the relative mobility based on the chromatograms obtained from the nanocapillaries under the elution pressure of 100 psi. In the plot, a notable feature is that DNA fragments elute before the void time of the nanocapillaries ($\bar{\mu}_L$ > 1), suggesting the fragments experiencing a greater mean axial speed than the elution buffer. An excellent fitting (R^2 ~ 0.997) of the experimental data to eqn (1) is observed for the scaling exponent ν = 0.5 with the resultant prefactor k = 78 nm kbp$^{-0.5}$ comparable to the value reported
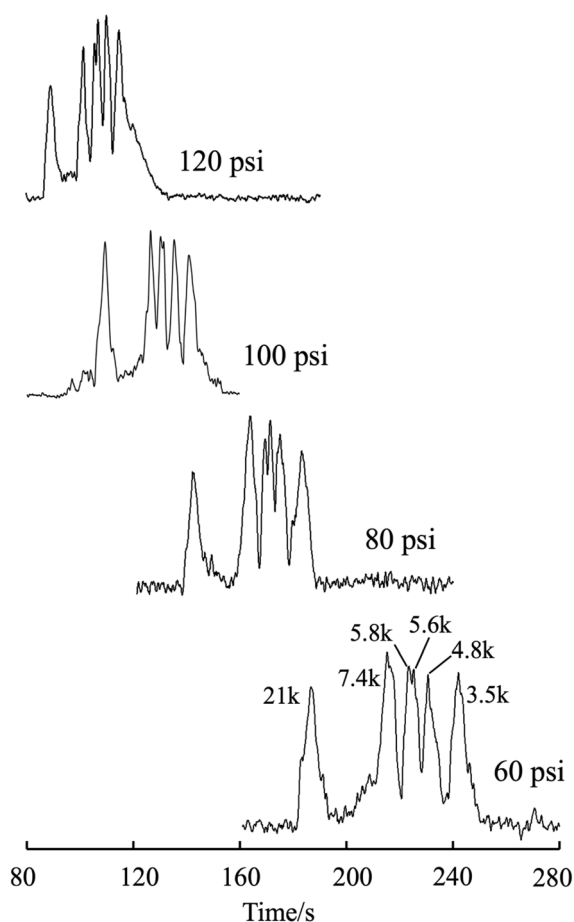

Fig. 4 Hydrodynamic chromatograms of a mixture of EcoRI-cut λ-phage DNA obtained from the microchip after a nearly 5 cm long separation run through the nanocapillaries at an elution pressure of 60, 80, 100, and 120 psi. Total DNA concentration in 10 mM TE buffer: ~50 μg mL^{-1}.
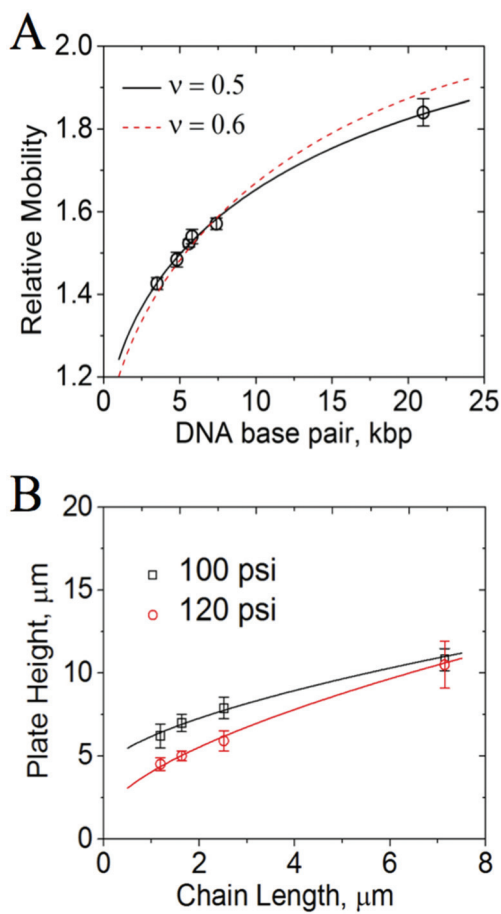
Fig. 5 Plots of (A) the relative mobility and (B) the plate height against the fragment length as per the chromatograms obtained from the nanocapillaries under the elution pressures of (A) 100 and (B) 100 and 120 psi (legend). The fitting curves are according to (A) eqn (1) and (B) eqn (2) with the scaling exponent set as (A) 0.5 and 0.6 (legend) and (B) 0.6. Error bars: ±1 s.d. (n = 5).

(79 nm kbp$^{-0.5}$) for hydrodynamic chromatography of DNA in fused-silica nanocapillaries (radius: 750 nm).[29] Nevertheless, in that study, eqn (1) did not return a good fitting for comparatively long DNA fragments (≳2 kbp) unless the right hand side of the equation contained an additional term that is proportional to L through a constant n. The authors attributed this term to deviations from the solid-sphere idealization of long fragments with their length further extending into the so-called "transition" region between those of a free-coiled state and a constant-mobility state.[29] In our study, despite the size of DNA fragments falling into the transition region and the capillary radius being comparable to that used in the aforementioned study, we found the consideration of such an extra term neither necessary for a quality fitting nor noticeably improved the existing fitting with the scaling exponent $\nu = 0.5$. However, with the exponent $\nu = 0.6$, including such an additional term nL with $n = 0.004$ transformed a comparatively poor fitting ($k = 64$ nm kbp$^{-0.6}$; $R^2 \sim 0.965$) into a reasonably good fitting ($k = 69$ nm kbp$^{-0.6}$; $R^2 \sim 0.994$).

Eqn (1) can be further refined according to the Dimarzio–Guttmann (DG) and Brenner–Gaydos (BG) theories: $\bar{\mu}_i = 1 + 2\lambda - C\lambda^2$ where C is the fitting parameter.[30] The increased quadratic term represents non-ideal effects such as the rotational motion of coiled fragments that results from such fragments being flanked by slow and fast streamlines (i.e., parabolic velocity profile). Again, we found no significant improvement in the fitting quality when we used the refined equation with $\nu = 0.5$ which resulted in a nearly unity C value, $C = 0.985$, and reduced the modified relation to eqn (1). However, we did see improvement with $\nu = 0.6$ ($k = 68.2$ nm kbp$^{-0.6}$; $C = 1.152$; $R^2 \sim 0.994$). These results collectively suggest that the DNA fragments can be treated here as ideal non-self-avoiding polymers with hydrodynamic radii $R_{HD} = 78N_{kbp}{}^{0.5}$, and the observed separation can be well described by the simple quadratic model of HDC.

Separation performance

For the same chromatograms and for those obtained at a slightly higher pressure (120 psi), the height equivalent of a theoretical plate, H, is shown as a function of chain length L in a plot shown in Fig. 5B. Depending on the chain length, H varies between ~4 and 10 μm, and the number of theoretical plates ranges from 100 000 to 250 000 plates per m. The separation efficiency could be further improved up to nearly million plates per m by integrating comparatively long nanocapillaries according to the fused-silica nanocapillary experiments.[35] In Fig. 5B, the measurements are fitted with the following relation:

$$H = A + \frac{\bar{u}R^2}{24D_c} \quad (2)$$

where A is a constant and D_c is the diffusion coefficient of DNA fragments. In the fittings, D_c is considered to be $cL^{-\nu}$ with the prefactor c treated as a fitting parameter along with A whereas the scaling exponent is set as $\nu = 0.6$ although excellent fittings ($R^2 > 0.990$) are provided with either value of ν. The resultant values of c and A are as listed in Table 1. It should be noted that L is taken here in the unit of μm and therefore c is in the unit of μm$^{2+0.6}$ s^{-1}.

It is noteworthy that eqn (2) deviates from the van Deemter relation, $H = A + B/\bar{u} + C\bar{u}$, where A, B, and C are constants signifying the terms that represent eddy diffusion, longitudinal diffusion, and resistance to analyte mass transfer between mobile and stationary phases, respectively. Although according to Golay, $A \approx 0$ for an open tubular liquid chromatography,[36]

Table 1 List of values as a result of the fittings shown in Fig. 5B according to eqn (2)

Elution pressure (psi)	ν	A	c	R^2
100	0.5	3.3	1.3	0.9959
	0.6	4.1	1.8	0.9933
120	0.5	0.1	1.2	0.9936
	0.6	1.2	1.6	0.9964

the constant found here is non-negligible except for $\nu = 0.5$ and 120 psi ($A \sim 0.1$ μm). This is also the case for the chromatograms obtained from open tubular fused-silica capillaries in a previous study where a nonzero A is attributed to the finite initial sample plug length or the finite detection window width.[35] Contrarily, the B term is negligibly small and thus omitted in eqn (2), signifying that the longitudinal diffusion is insignificant as previously demonstrated in fused-silica capillaries.[31,35]

DNA diffusivity under confinement

Fig. 6 shows a log–log plot of the diffusion coefficient D_c against the fragment length L from the fittings according to eqn (2). The plot also includes the self-diffusion coefficient previously reported for isolated DNA fragments in bulk solution (D_{bulk}).[37] Despite comparable slopes, the diffusion coefficients derived here are lower than the bulk values by a scaling factor of 0.7–0.8. This is in agreement with previous studies which reveal that DNA or polymer fragments confined in a capillary or a slit exhibit a reduced self-diffusion coefficient (D_c) because fragments experience a higher viscous drag due to their conformational changes (e.g. elongation, lateral expansion).[38] Stein et al., in particular, measured the scaling factor for the self-diffusivity of λ-DNA molecules confined in a slit and reported the measured results in a plot against the normalized height R_G/h with R_G being the radius of gyration.[19] Considering the normalized diameter ranged here from ∼0.1 to 0.3 (h the capillary diameter; R_G ∼100 to ∼300 nm), the reported plot yields a scaling factor of 0.6 to 0.8 in this range, which concurs with those derived from Fig. 6. Nevertheless, this is only a rough comparison because it omits molecule–molecule interactions between DNA fragments.
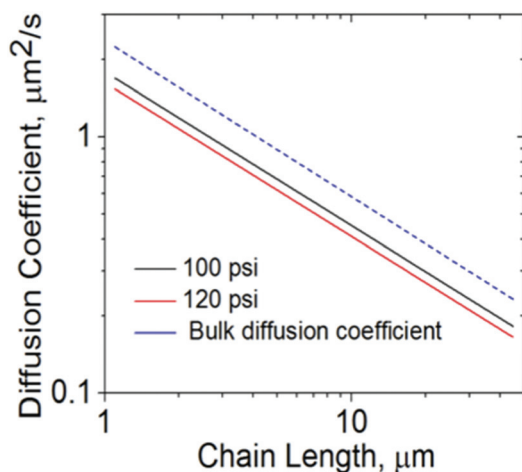

Fig. 6 Log–log plots of the diffusion coefficient against the fragment length as per the fittings of plate height according to eqn (2) with the scaling exponent set as 0.6 (Fig. 5B). The dashed line describes the self-diffusion coefficient previously reported for isolated DNA fragments in bulk solution.[33]

Further validation of the model

Lastly, we compare the R_{HD} values obtained from the mobility fittings (Fig. 5A) to those derived from the reduced diffusivity estimates D_c based on the plate height fittings (Fig. 5B). Assuming good solvent conditions and the Zimm model, R_{HD} is related to D_c through the following expressions:[37,39]

$$R_{HD} = 0.64 R_G$$
$$R_G = 0.196 k_B T / \sqrt{6} \mu D_c$$

(3)

where k_B is the Boltzmann constant, and T and μ are the solvent temperature (in K) and viscosity. After substituting $D_c \sim cL^{-0.6}$, eqn (3) can be summarized as $R_{HD} \sim k'L^{0.6}$ with k' being 118 nm μm$^{-0.6}$ for the c value obtained with the elution pressure of 100 psi (Table 1). For the same elution pressure, the mobility fitting by the simple quadratic model featuring an increased quadratic term results in the relation $R_{HD} \sim kN_{kbp}^{0.6}$ with k being 68 nm kbp$^{-0.6}$ as stated above. This leads to the ratio $k'/k \sim 1.73$ μm$^{-0.6}$ kbp$^{0.6}$, which is close enough to 1.91 μm$^{-0.6}$ kbp$^{0.6}$, the value required to uphold the well-known relation for the scale conversion factor $L/N_{kbp} \sim 0.34$ μm kbp^{-1}.[40] This concludes that comparable hydrodynamic radii are estimated using two separate model fittings to the experimental measurements (mobility and plate height), further establishing HDC as the separation mechanism in the nanocapillaries.

Conclusions

We have developed a robust HDC microchip for pressure-driven separation of DNA and further established the separation mechanism, demonstrating that the simple quadratic HDC model is well applicable to the experimental data reasonably predicting the relative mobility of DNA in relation to DNA length. The silicon microchip presents a highly regular array of bare glass nanocapillaries integrated through low-resolution photolithography and standard semiconductor processing techniques. Like fused-silica counterparts, the nanocapillaries feature a cylindrical interior and maintain a uniform profile over a separation run of centimeters. However, unlike fused-silica counterparts, the nanocapillaries support pressure-driven transport characteristics of DNA that can be well explained by the simple quadratic model without any modification required (e.g. no extra term), at least when $\nu = 0.5$. Model fittings to the mobility and plate height data independently yield comparable results, both fittings predicting larger hydrodynamic radii and smaller diffusion coefficients than those of the corresponding isolated fragments measured while being unconfined in bulk solution. Given the crowding effect of DNA here, it is intriguing to find that the scaling factor brought by physical confinement is within the range of those experimentally measured on isolated single DNA coils.

Future research shall focus on improving the performance and matching the performance of those achieved by fused-silica nanocapillaries, which offer a separation run far longer,

at least an order of magnitude, than those integrated here. We believe that the integration of long nanocapillaries is within the realm of the fabrication process described here and limited only by the available area on the silicon wafer. Challenges such as randomly occurring defects during photolithography or incomplete nanocapillary fillings due to trapping of gas bubbles can be simply addressed by adopting a redundancy in design, *i.e.*, integrating a massive array of nanocapillaries. However, challenges remain to be addressed include the handling of a high separation pressure demand by relatively long nanocapillaries and the sourcing of such high pressure through means compatible with the microchip settings. This is true in particular for accelerating the DNA separation process to render the HDC microchip competitive with electrophoretic counterparts such as those featuring three-dimensional nanowires.[12]

Acknowledgements

References

1 B. A. Roe, J. S. Crabtree and A. S. Khan, *DNA isolation and sequencing*, Wiley-Blackwell, 1996.

2 Y. Kim and M. D. Morris, *Anal. Chem.*, 1994, **66**, 3081–3085.

3 J. Sudor and M. V. Novotny, *Anal. Chem.*, 1994, **66**, 2446–2450.

4 Y. S. Kim and M. D. Morris, *Anal. Chem.*, 1995, **67**, 784–786.

5 X. Y. Wang, L. Liu, W. Wang, Q. S. Pu, G. S. Guo, P. K. Dasgupta and S. R. Liu, *TrAC, Trends Anal. Chem.*, 2012, **35**, 122–134.

6 B. M. Olivera, P. Baine and N. Davidson, *Biopolymers*, 1964, **2**, 245–257.

7 W. D. Volkmuth and R. H. Austin, *Nature*, 1992, **358**, 600–602.

8 D. Nykypanchuk, H. H. Strey and D. A. Hoagland, *Science*, 2002, **297**, 987–990.

9 W. D. Volkmuth, T. Duke, M. C. Wu, R. H. Austin and A. Szabo, *Phys. Rev. Lett.*, 1994, **72**, 2117–2120.

10 N. Kaji, Y. Tezuka, Y. Takamura, M. Ueda, T. Nishimoto, H. Nakanishi, Y. Horiike and Y. Baba, *Anal. Chem.*, 2004, **76**, 15–22.

11 Y. Zeng and D. J. Harrison, *Anal. Chem.*, 2007, **79**, 2289–2295.

12 S. Rahong, T. Yasui, T. Yanagida, K. Nagashima, M. Kanai, G. Meng, Y. He, F. Zhuge, N. Kaji, T. Kawai and Y. Baba, *Sci. Rep.*, 2014, **5**, 10584–10592.

13 J. Han and H. G. Craighead, *Science*, 2000, **288**, 1026–1029.

14 Z. Cao and L. Yobas, *Anal. Chem.*, 2014, **86**, 737–743.

15 Z. Cao and L. Yobas, *ACS Nano*, 2015, **9**, 427–435.

16 J. Tang, N. Du and P. S. Doyle, *Proc. Natl. Acad. Sci. U. S. A.*, 2011, **108**, 16153–16158.

17 N. P. Teclemariam, V. A. Beck, E. S. G. Shaqfeh and S. J. Muller, *Macromolecules*, 2007, **40**, 3848–3859.

18 W. Reisner, N. B. Larsen, H. Flyvbjerg, J. O. Tegenfeldt and A. Kristensen, *Proc. Natl. Acad. Sci. U. S. A.*, 2009, **106**, 79–84.

19 D. Stein, F. H. J. van der Heyden, W. J. A. Koopmans and C. Dekker, *Proc. Natl. Acad. Sci. U. S. A.*, 2006, **103**, 15853–15858.

20 X. Y. Wang, V. Veerappan, C. Cheng, X. Jiang, R. D. Allen, P. K. Dasgupta and S. R. Liu, *J. Am. Chem. Soc.*, 2010, **132**, 40–41.

21 X. Y. Wang, J. Z. Kang, S. L. Wang, J. J. Lu and S. R. Liu, *J. Chromatogr., A*, 2008, **1200**, 108–113.

22 K. J. Liu, T. D. Rane, Y. Zhang and T. H. Wang, *J. Am. Chem. Soc.*, 2011, **133**, 6898–6901.

23 N. Iki, Y. Kim and E. S. Yeung, *Anal. Chem.*, 1996, **68**, 4321–4325.

24 C. S. Effenhauser, A. Manz and H. M. Widmer, *Anal. Chem.*, 1993, **65**, 2637–2642.

25 L. Duan, Z. Cao and L. Yobas, *Anal. Chem.*, 2016, **88**, 11601–11608.

26 Y. F. Liu and L. Yobas, *Biomicrofluidics*, 2012, **6**, 046502.

27 H. Shimizu, K. Morikawa, Y. Liu, A. Smirnova, K. Mawatari and T. Kitamori, *Analyst*, 2016, **141**, 6068–6072.

28 R. Ishibashi, K. Mawatari, K. Takahashi and T. Kitamori, *J. Chromatogr., A*, 2012, **1228**, 51–56.

29 X. Y. Wang, L. Liu, Q. S. Pu, Z. F. Zhu, G. S. Guo, H. Zhong and S. R. Liu, *J. Am. Chem. Soc.*, 2012, **134**, 7400–7405.

30 R. Tijssen, J. Bos and M. E. Vankreveld, *Anal. Chem.*, 1986, **58**, 3036–3044.

31 L. Liu, V. Veerappan, Q. S. Pu, C. Cheng, X. Y. Wang, L. P. Lu, R. D. Allen and G. S. Guo, *Anal. Chem.*, 2014, **86**, 729–736.

32 P. J. Flory, *Principles of polymer chemistry*, Cornell University Press, 1953.

33 D. W. Schaefer, J. F. Joanny and P. Pincus, *Macromolecules*, 1980, **13**, 1280–1289.

34 A. Dobay, J. Dubochet, K. Millett, P. E. Sottas and A. Stasiak, *Proc. Natl. Acad. Sci. U. S. A.*, 2003, **100**, 5611–5615.

35 Z. F. Zhu, L. Liu, W. Wang, J. J. Lu, X. Y. Wang and S. R. Liu, *Chem. Commun.*, 2013, **49**, 2897–2899.

36 M. J. E. Golay, in *Gas Chromatography*, ed. D. H. Desty, Academic Press, New York, 1956, p. 36.

37 D. E. Smith, T. T. Perkins and S. Chu, *Macromolecules*, 1996, **29**, 1372–1373.

38 F. Brochard and P. G. Degennes, *J. Chem. Phys.*, 1977, **67**, 52–56.

39 C. M. Kok and A. Rudin, *Makromol. Chem., Rapid Commun.*, 1981, **2**, 655–659.

40 J. D. Watson and F. H. Crick, *Nature*, 1953, **171**, 737–738.